Inverted plasmonic lens design for nanometrology applications

OPEN ACCESS
IOP Publishing
Measurement Science and Technology
Meas. Sci. Technol. **31** (2020) 074013 (10pp)
https://doi.org/10.1088/1361-6501/ab7e6b

Inverted plasmonic lens design for nanometrology applications

T Käseberg[1], T Siefke[1,2], S Kroker[1,3] and B Bodermann[1]

[1] Physikalisch-Technische Bundesanstalt, Bundesallee 100, 38116 Braunschweig, Germany
[2] Friedrich-Schiller-Universität Jena, Abbe Center of Photonics, Institute of Applied Physics, Max-Wien-Platz 1, 07743 Jena, Germany
[3] Laboratory for Emerging Nanometrology, Technische Universität Braunschweig, 38092 Braunschweig, Germany

E-mail: tim.kaeseberg@ptb.de

Received 21 December 2019, revised 6 March 2020
Accepted for publication 10 March 2020
Published 4 May 2020

Abstract

Planar plasmonic lenses have attracted a great deal of interest over the last few years for their super-resolution focusing capabilites. These highly compact structures with dimensions of only a few micrometres allow for the focusing of light to sub-wavelength-sized spots with focal lengths reaching into the far-field. This offers opportunities for new methods in nanometrology; for example, applications in microscopic Mueller matrix ellipsometry setups. However, the conventional plasmonic lens is challenging to fabricate. We present a new design for plasmonic lenses, which is called the inverted plasmonic lens, to accommodate the lithographic fabrication process. In this contribution, we used numerical simulations based on the finite element method in combination with particle swarm optimization to determine ideal parameter ranges and tolerances for the design of inverted plasmonic lenses for different wavelengths in the visible and near-infrared domain and focal lengths between 5 μm and 1 mm.

Keywords: plasmonic lenses, ellipsometry, numerical simulations, metrology

(Some figures may appear in colour only in the online journal)

1. Introduction

Since their first descriptions in the early 2000s [1–3], planar plasmonic lenses have attracted a great deal of interest for their promising qualities in applications such as optoelectronics, nanolithography and, especially, super-resolution focusing [4–6]. Plasmonic lenses, only consisting of a metallic slab with a plasmonic metasurface, are highly compact structures with dimensions of only a few micrometers, which allows for the focusing of light to spot sizes below the wavelength of the incident light with focal lengths reaching into the far-field [7]. This offers opportunities for the realization of new techniques for the characterization of nanostructures. Common optical methods like microscopy are naturally non-invasive and fast, but limited by diffraction. Beyond that, super-resolution techniques like stimulated emission depletion microscopy (STED) or stochastic optical reconstruction microscopy (STORM) are often viable for biological applications only, as they rely on fluorophores being present or being implemented on the sample [8, 9]. In addition, ellipsometry is an optical measurement technique that is already in use to characterize nanostructures [10, 11]. In particular, spectroscopic Mueller matrix ellipsometry is a versatile but still auspicious tool for the optical characterization of structured surfaces. The combination of Mueller matrix ellipsometry with microscopic methods has revealed additional topological information in off-diagonal elements of the Mueller matrix that are useful for classifying the shape of the structures [12, 13]. Therefore, using plasmonic lenses as a focusing tool in ellipsometry is a promising way to efficiently characterize nanostructured samples. The lenses could be implemented in

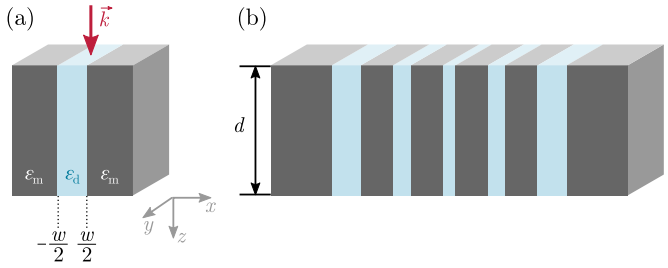

Figure 1. Schematics of (a) a metal–dielectric–metal waveguide and (b) a plasmonic lens, formed by placing waveguides of different widths next to each other. Blue indicates dielectric material, grey indicates metal. The red arrow shows the direction of the incident light.

ellipsometric setups similar to the tips used in near-field scanning optical microscopy (NSOM) to create sub-wavelength-sized field enhancement that could be used to scan the sample to produce high-resolution Mueller matrix images. For this application, plasmonic lenses that generate small focal spots with high intensities are required. As the area of application of a plasmonic lens is limited to a single combination of wavelength and focal length, many lenses with varying parameters have to be fabricated. However, the conventional planar plasmonic lens, which is formed by nanoscaled slits in a thick metallic slab, is challenging to fabricate. Common fabrication techniques require complex setups and are limited in their choice of materials. Because of that, in this contribution, we present a new design of a plasmonic lens with an inverted geometry that is easier to fabricate with lithographic methods. We discuss the inverted plasmonic lens design as well as the optimization of different parameters that influence its functionality.

1.1. Plasmonic lenses

Plasmonic lenses are based on the propagation behaviour of surface plasmon polaritons (SPPs) through metal–dielectric–metal waveguides. SPPs are the quasiparticles of surface electron density fluctuations, coupled to the photons that excited them. They are inherently transverse magnetic (TM) polarized electromagnetic waves that can only be excited at interfaces between materials with a positive and a negative permittivity, respectively; for example, a dielectric and a metal. They travel along such an interface and decay at a distance from their point of excitation [14–16].

Consider a rectangular dielectric waveguide with the width w surrounded by two parallel metallic plates as depicted in figure 1(a). The plates are infinitely extended in the y-direction. The electromagnetic field propagates along the z-direction and is confined in the x-direction. For this geometry, a characteristic equation can be formulated [15, 17]

$$\tanh\left(\frac{w}{2}\sqrt{\beta^2-k_0^2\varepsilon_d}\right)=-\frac{\varepsilon_d}{\varepsilon_m}\frac{\sqrt{\beta^2-k_0^2\varepsilon_m}}{\sqrt{\beta^2-k_0^2\varepsilon_d}} \qquad (1)$$

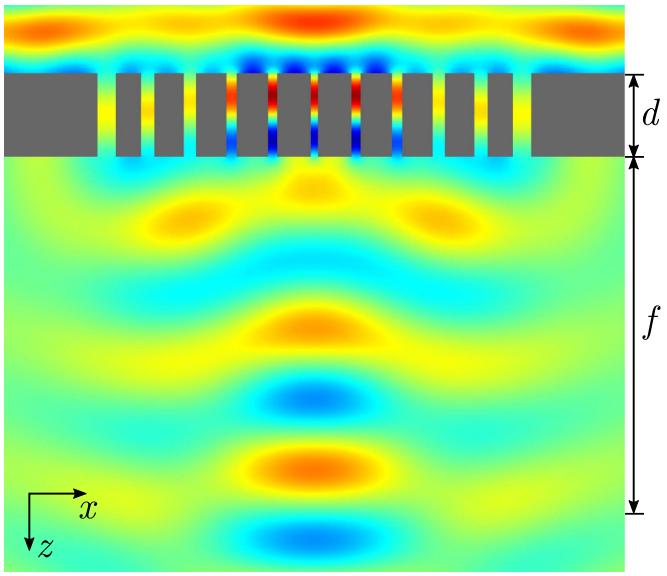

Figure 2. Plasmonic lens, illuminated from above by a plane wave. The different widths of the slits generate a phase delay distribution that curves the wavefront and creates a focal spot.

that depends on the width w, the complex permittivities $\varepsilon_{m,d} = \varepsilon_{m,d}' + i\varepsilon_{m,d}''$ of the materials, and the propagation constant β, which is equivalent to the wavenumber of the SPPs and describes the propagation as well as the damping along the direction of propagation [14]. The most fundamental case for such a waveguide would be a slit in a metallic slab. In this case, air plays the role of the dielectric medium. As can be seen from the characteristic equation (1), the propagation of the SPPs through such a slit or waveguide depends on its width w. By carefully choosing an array of these waveguides with different widths, as suggested in figure 1(b), the transmitted wavefront on the other side of the slab can be altered. The characteristic equation is easily solved for the width w of a single slit:

$$w=\frac{2}{\sqrt{\beta^2-k_0^2\varepsilon_d}}\tanh^{-1}\left(-\frac{\varepsilon_d\sqrt{\beta^2-k_0^2\varepsilon_m}}{\varepsilon_m\sqrt{\beta^2-k_0^2\varepsilon_d}}\right). \qquad (2)$$

As Shi *et al* pointed out, changes of the phase ϕ of the light at transmission through a dielectric layer depend mostly on the propagation constant β [2]: where d is the length of the slit or the thickness of the metallic slab, respectively. Considering an arrangement of slits through a metallic slab along the x-axis like in figure 2, we want to choose slit widths that cause a phase delay which results in a focal spot at a distance f from the slab, just like an optical lens. Therefore, the phase delay in the centre of the lens has to be the largest, followed by smaller delays with increasing distance from the centre along the x-axis. To achieve this, the phase distribution of the plasmonic lens is supposed to be [2]: where $m \in \mathbb{N}$. By comparing this with equation (3), we obtain an expression for the propagation constant $\beta(x) = \phi(x)/d$ depending on the position x of the slit on the metallic slab. This can be used in equation (2) to formulate an expression for the slit width $w(x)$ depending on the slit position. As an example, the phase distribution $\phi(x)$ and

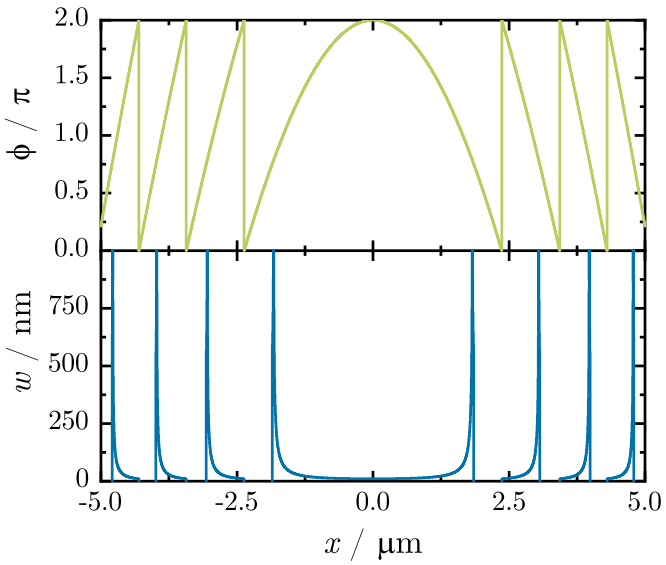

Figure 3. Phase distribution $\phi(x)$ (green) and corresponding slit width $w(x)$ (blue) to achieve the phase delay. Example for a plasmonic lens (iridium and air) with $d = 200$ nm and $f = 5$ μm at $\lambda_0 = 532$ nm.

the corresponding slit widths $w(x)$ are plotted in figure 3 for a plasmonic lens with a thickness of 200 nm, a wavelength of 532 nm and a focal length of 5 μm. With increasing distance from the centre, the slit width increases. The sudden decrease of the width in the plot is explained by numerical issues due to exponentially increasing values that eventually exceed the floating-point range. Note that due to the 2π periodicity of ϕ, slits do not get increasingly larger but periodically jump back to smaller widths in a Fresnel lens-like manner.

$$\phi = \beta d, \tag{3}$$

$$\phi(x) = 2\pi m + \frac{2\pi f}{\lambda_0} - \frac{2\pi\sqrt{f^2 + x^2}}{\lambda_0}, \tag{4}$$

1.2. Common fabrication techniques

As discussed in section 1.1, we can realize a plasmonic lens by fabricating either an array of slits in a metallic slab or a sequence of metallic and dielectric layers of certain widths. One could easily think of the latter method as depositing alternating layers of metal and dielectric on top of each other. However, this would result in very large thicknesses d that would not allow for the SPPs to propagate all the way through the lens, or would require further postprocessing which could affect its functionality. Additionally, constructing these consecutive layers or just the metallic sidewalls from the bottom up is a complicated task. This is presumably the reason why plasmonic lenses are usually produced using top-down approaches, the most common being focused ion beam (FIB) milling [4, 18–20]. These approaches are required to produce slits of a few tens of nanometres in width in metallic sheets with thicknesses up to a few micrometres, depending on the application wavelength.

SPPs can only be excited at interfaces between materials with a positive and a negative permittivity, respectively. In order to define a materials optical performance regarding SPPs, a quality factor has been formulated [21]: higher values of Q_{SPP} indicate a better plasmonic performance of the corresponding material. For example, the currentbest pure metal and therefore most common material for plasmonic applications is silver (Ag) with a quality factor of $Q_{\mathrm{SPP}} \approx 373$ at a wavelength of 532 nm (data from [22]). Similarly, metals like aluminum (Al), copper (Cu) and gold (Au) also present high-quality factors [23].

$$Q_{\mathrm{SPP}} = \frac{\varepsilon_{\mathrm{m}}'^2}{\varepsilon_{\mathrm{m}}''}. \tag{5}$$

2. Inverted plasmonic lens design

We can use a combination of equations (2)–(4) to design plasmonic lenses with nearly arbitrary dimension and properties. However, the conventional plasmonic lens, being a metallic slab with dielectric slits, is rather challenging to fabricate and requires specialized instrumentation, as mentioned in section 1.2. While FIB milling is only suited for the fabrication of small quantities of samples for research purposes, etching techniques allow for a fast and reliable production of many structures with desired parameters. However, purely metallic structures with such high aspect ratios are very challenging to produce without large deviations and in the high quantities that would be needed to make the application of plasmonic lenses easily accessible. For this reason, we designed a new kind of plasmonic lens to comply with the electron beam lithography fabrication process. Figure 4 shows a comparison between the classic design in figure 4(a) and our design in figure 4(b). In the conventional design, SPPs travelled along the metal–dielectric–interface through a slit in a metallic slab. In our inverted design, however, they travel through dielectric ridges instead of slits. These ridges are coated with a metallic layer to create the interface needed for the propagation. A metallic cap on the substrate ensures that light transmits through the ridges only. Because of the inversion from slits to ridges, we call this design the inverted plasmonic lens. This design can be realized by fabricating dielectric ridges in an electron beam lithography process, coating the ridges with metal using atomic layer deposition (ALD) and then removing the coating from the top of the ridges, similar to the production of wire grid polarizers [24]. This process mitigates the issue of etching metal with high aspect ratios by replacing the metal etch process by an inherently well-controllable ALD deposition process. An example of the field of an inverted plasmonic lens producing a focal spot is depicted in figure 5(b) in comparison to the field of a conventional plasmonic lens in figure 5(a).

2.1. Materials

For the designs in this contribution, we used iridium (Ir) as metallic component. At 532 nm wavelength, Ir has a quality

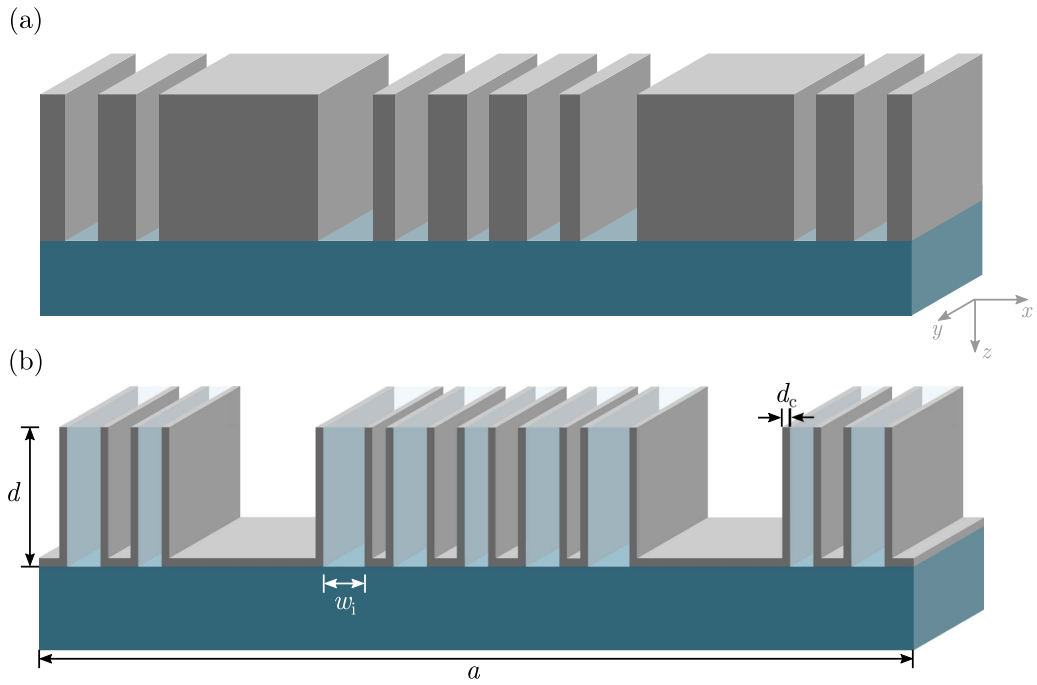

Figure 4. Schematics of (a) a conventional plasmonic lens and (b) an inverted plasmonic lens. Dark blue indicates the substrate material, grey stands for metal and transparent light blue indicates dielectric material (resist).

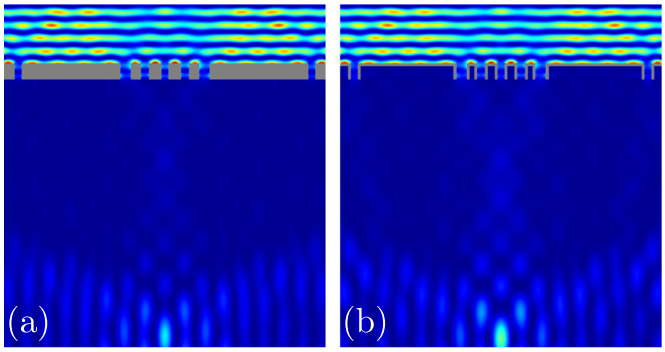

Figure 5. Intensity distribution of a conventional (a) and an inverted plasmonic lens (b), illuminated from above, for the same geometrical parameters. Both designs produce a focal spot in the desired distance from the lens. After optimizing the structure, the focal spot of the inverted design has about 10% higher intensity compared to the conventional design. Images cropped to area of interest.

factor of $Q_{\mathrm{SPP}}(\mathrm{Ir}) \approx 9.67$ (data from [25]), which is well below the values of the other materials mentioned in section 1.2. We chose Ir because it still presents a decent optical performance while being very resistant to oxidation compared to Ag or Al, which leads to an enhanced durability of the lens. Additionally, iridium has already been used successfully as a material for wire grid polarizers which work in the same spectral range and present a similar geometrical structure compared to plasmonic lenses [26]. As dielectric material, air would be well suited, but difficult to realize. Therefore, we chose the AZ1505 photoresist by MicroChemicals which is easily processed during lithography. The resist has a refractive index of about 1.65 in the visible and near-infrared range. This is slightly higher than the refractive index of SiO_2, which is considered as a substrate material.

2.2. *Parameter optimization*

In a preliminary design [13], only a poor optical performance of the inverted plasmonic lens compared to conventional plasmonic lenses could be achieved. For the same range of focal lengths, the inverted lenses showed larger focal spots with smaller intensities than in the conventional design. Since structural parameters critically influence performance, we carried out further numerical simulations using the finite element method (FEM) tool JCMwave [27], supported by particle swarm optimization (PSO).

PSO is a stochastic global optimization algorithm used to find the best solution to a multidimensional problem in a given parameter space [28]. It is based on the behaviour of animals such as fish or birds in large groups. In each iteration of the algorithm, statistically distributed particles update their position in the parameter space by using their velocity vector. This vector is composed of three terms: the particle's inertia, their knowledge of their own best position in the parameter space so far and of the group's best position so far. Depending on the weighting of each of these hyperparameters, some particles explore the parameter space whereas other particles flock together. Eventually, depending on the size of the swarm and the maximum number of iterations, the whole particle swarm will converge into an optimum. For an improved control over the swarm dynamics, we applied constriction coefficients as proposed by Clerc and Kennedy [29]. As the selection of ideal hyperparameters is an optimization problem itself,

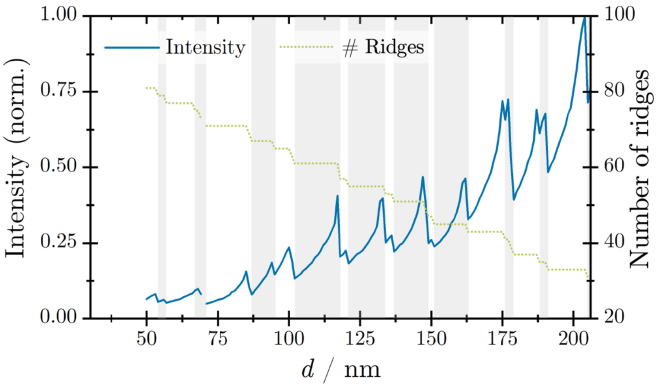

Figure 6. Intensity of the focal spot (blue, solid) and number of ridges (green, dotted) of a lens with focal length $f = 10$ µm at $\lambda_0 = 532$ nm when evaluating equation (2) for different thicknesses d. The grey striped background highlights changes of the number of ridges.

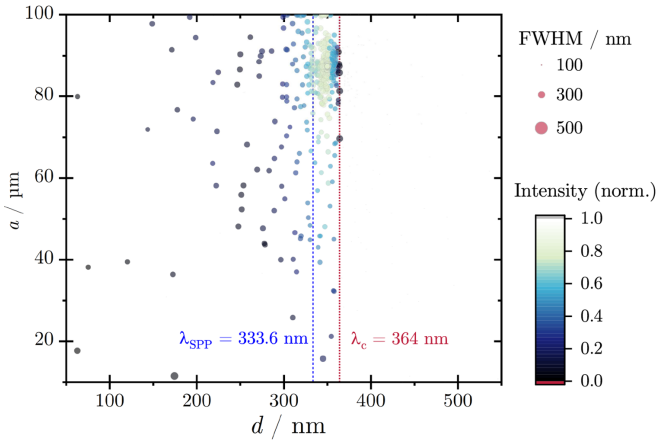

Figure 7. Results of the PSO of an inverted plasmonic lens consisting of iridium and SiO_2 with $f = 5$ µm for apertures a between 10 and 100 µm and thicknesses d between 50 and 550 nm at $\lambda_0 = 532$ nm. The swarm consisted of 35 particles in 35 iterations. Size of the dots indicates FWHM, hue indicates intensity. The blue dashed line shows the wavelength of the SPPs λ_{SPP}, the red dotted line shows the cut-off wavelength λ_c.

common default values were used that are known to yield appropriate results.

Optimization of three different parameters using this method was carried out: Thickness of the ridges d, coating thickness d_c and aperture a (maximum extent of the lens in x-direction, compare figure 4). The objective function of the optimization algorithm is to minimize the ratio between full width at half maximum (FWHM) and intensity of the focal spot in order to improve the performance of the lens. Larger intensities and smaller spot sizes evaluate to smaller values of the objective function and are therefore more desirable for the particles. This way, we can outperform the preliminary design which achieved only a poor optical performance.

Due to the high computational costs evoked by the evaluation of each particle's position with the FEM, the optimization could not be performed for arbitrary sets of wavelength and focal length. For these reasons, optimization was only performed for some parameter sets to show the general behaviour of the inverted plasmonic lens and to find regions in the parameter space that lead to reliable designs. Most optimizations were performed for wavelengths of 455 nm or 532 nm and focal lengths of 5–10 µm to keep computational costs low. Usually, convergence was reached already after about 30–40 iterations with 20–30 particles. Higher swarm sizes or more iterations were not feasible because the evaluation of a single particle's position corresponds to a FEM simulation that takes between 5 and 15 minutes on our computation system, depending on the current parameter set, which leads to computation times of up to 2 weeks. Note that the following discussions concern the inverted plasmonic lens design in particular, but are also valid for the classic design in general.

3. Optimization results

In the following, we discuss the optimization of the thickness d (height of the ridges), the coating thickness d_c, the aperture a and the kind of ridge arrangement for inverted plasmonic lenses according to the methods presented in section 2.

3.1. Ridge height

Based on equations (2)–(4), the blue solid curve in figure 6 shows the intensity of the resulting focal spot when computing the set of ridge widths for different thicknesses d up to 200 nm and simulating the plasmonic lenses with these parameters. The intensity increases with larger thickness, but occasionally falls back to lower values. This can be explained by comparing the intensity with the number of ridges, illustrated by the green dotted plot in figure 6. As the thickness increases, the general width of the ridges also increases due to equation (2) and the propagation constant β being inversely proportional to d. Larger widths lead to a higher throughput and therefore higher intensity of the focal spot. However, the number of ridges that fit into the fixed aperture is limited. Also, adjacent ridges limit each other in size. Therefore, ridges that are too large must occasionally be removed from the design to have a physically realizable lens. Each time one or several ridges are removed, the intensity drops drastically because the throughput is reduced, as can be observed in figure 6.

The intensity curve has a maximum at a thickness slightly above the wavelength of the SPPs λ_{SPP} as presented in figure 7. It depicts a PSO performed over thickness and aperture with 35 particles in 35 iterations. Each point in the plot corresponds to one evaluation of a particle, regardless of the iteration. Their size is proportional to the FWHM of the focal spot, while their hue represents the intensity, with lighter dots showing higher intensities. The swarm converged around $d = 350$ nm and $a = 87$ µm. The FWHM of each evaluation was below the incident wavelength, with a mean FWHM of around 190 nm. Most of the evaluations took place for thicknesses greater than $\lambda_{SPP} = 333.6$ nm [16]. However, each evaluation attempted for d greater than $\lambda_c = \lambda_0/n_d = 364$ nm failed, where n_d is the refractive index of the dielectric material. This cut-off is comprehensible when taking a look at the square root in equation (2) (assuming $n_d \approx \sqrt{\varepsilon_d}$): When $d \geq \lambda_0/n_d$, the radicand

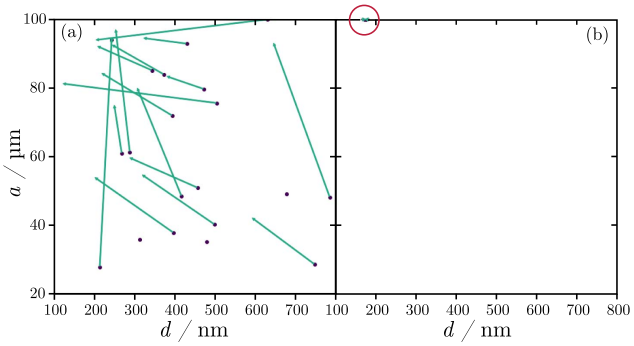

Figure 8. Particle swarm optimization with a fixed parameter set for $f = 5$ µm at $\lambda_0 = 455$ nm with 20 particles in 35 iterations over thickness d and aperture a, after first iteration (a) and after last iteration (b). The ridge widths and positions were computed beforehand for $d = 200$ nm. Dark blue dots indicate the position of the particles in the parameter space, green arrows represent their velocity. Some velocity vectors are not plotted due to overshooting out of the parameter space. The red circle highlights the clustering of the swarm at the end.

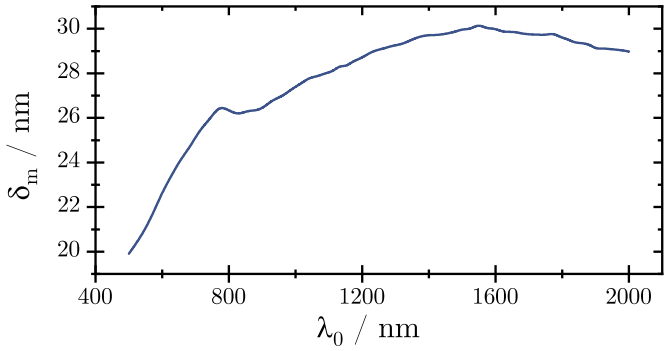

Figure 9. Penetration depth δ_m of SPPs into Ir for visible and infrared wavelengths. Computed with data from [25].

is negative for every value of $\phi(x)$, so the square root always yields a complex result. This leads to $w(x)$ taking on complex values that are physically not realizable. These results suggest that for optimal performance, the set of ridge widths and positions should be computed for thicknesses between λ_{SPP} and λ_c.

$$\sqrt{\beta(x)^2 - k_0^2 \varepsilon_d} = \sqrt{\frac{\phi(x)^2}{d^2} - \frac{4\pi^2 n_d^2}{\lambda_0^2}}. \tag{6}$$

In addition to re-evaluating equation (2) for each thickness, we also optimized the thickness for fixed sets of ridge widths and positions by computing the parameter set only once for a single thickness and then simulating the lens with these parameters while varying the thickness and aperture. Figure 8 shows the first and the last iteration of a PSO with fixed ridge parameters. The particles are randomly distributed over the parameter space in the beginning. After the first iteration, their velocity vectors mostly point towards the upper-left corner of the parameter space. That indicates the position of the optimum at small thicknesses and large apertures. This assumption proves to be true regarding the end of the algorithm in figure 8(b). The particles collected in the upper-left corner and the best evaluation of the objective function was found at $d = 172$ nm and $a = 100$ µm. We will discuss the aperture in section 3.4. The result for the thickness lies below the thickness of $d = 200$ nm for which the lens was designed. The reason for this behaviour will be discussed in section 4.2.

3.2. Coating thickness

As SPPs travel along a metal–dielectric interface, they penetrate both media to a certain extent, which is considered by the penetration depths δ_m and δ_d, respectively [16]. Figure 9 shows the penetration depths δ_m of SPPs into iridium for different wavelengths in the visible and infrared regime. At no point does δ_m exceed 30 nm. The SPPs inside the dielectric waveguide are expected to couple, but they should not be able to couple to the SPPs in adjacent ridges to prevent interactions. Additionally, equation (2) is only valid for independent waveguides, so the ridges must not be coupled. Therefore, the metallic spacing between two ridges should be at least as thick as the penetration depth of the SPPs into the metal [3, 16].

The penetration depth is $\delta_m \approx 21$ nm at a wavelength of 532 nm. For this wavelength, figure 10 depicts the intensity and FWHM of the focal spot for a lens with a fixed set of ridge positions and widths, but for varying coating thicknesses d_c. The intensity reaches its maximum at $d_c = 28$ nm, which is larger than δ_m. However, for larger thicknesses, the intensity decreases. One explanation for this behaviour is that SPPs may penetrate through thinner metallic layers and couple into the dielectric filling between the ridges. There they are able to transform back to propagating waves which interfere with the desired propagation through the ridges and contribute to the overall intensity in the focal plane. So it is misleading to trust only the intensity when deciding for a coating thickness. Eventually, an increase of d_c would lead to a convergence towards the classic design, and the intensity should stabilize. The decrease towards lower thicknesses can also be explained by a too thin d_c as SPPs penetrate easily through the coating and no real propagation can be formed. Concerning the FWHM, a minimum of about 194 nm can be found at $d_c = 51$ nm. Nevertheless, the FWHM remains mostly constant for coating thicknesses larger than the penetration depth.

The optimization of the coating thickness for a lens with a focal length of 5 µm at a wavelength of 532 nm is illustrated in figure 11, where the initial state of the particle swarm is presented in figure 11(a). The parameter space consists of the thickness of the ridges d as well as the coating thickness d_c. After 40 iterations, the swarm reached the state presented in figure 11(b). Concerning the thickness, the swarm converged in $d \approx 327$ nm, which again lies below λ_{SPP}. In regard of the penetration depth of SPPs into the metal, a lower bound of 20 nm for the coating thickness was chosen. However, the swarm tended towards this limit and collected at the lower bound of the parameter space, as highlighted in figure 11(b). This is due to the effects already observed in figure 10. The algorithm tries to optimize the intensity of the focal spot in relation to its FWHM. Thus, a higher intensity is desirable for the swarm,

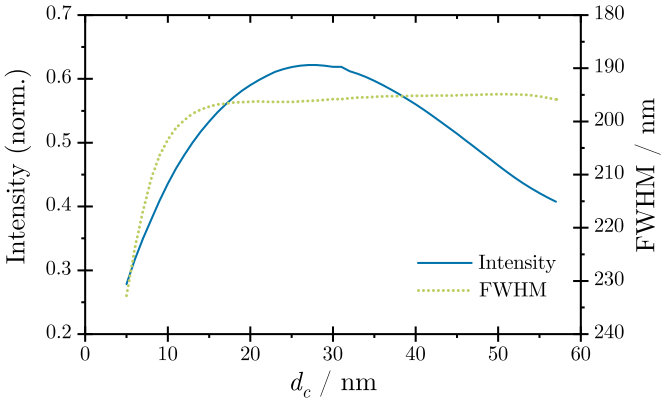

Figure 10. Intensity (blue, solid) and FWHM (green, dotted) in dependence of the coating thickness for a lens with $f = 5$ µm and $\lambda_0 = 532$ nm.

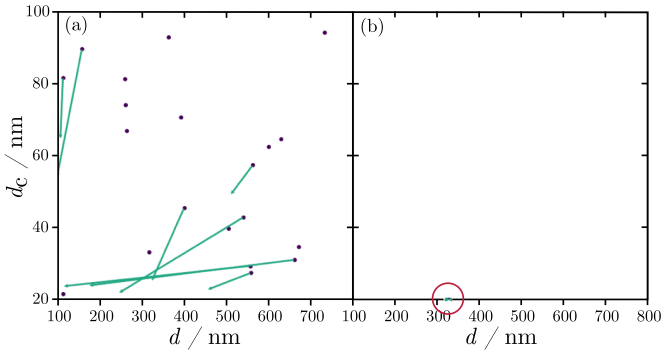

Figure 11. Particle swarm optimization with 20 particles over thickness d and coating thickness d_c, after first iteration (a) and after last iteration (b). Some velocity vectors are not plotted due to overshooting out of the parameter space. The red circle highlights the clustering of the swarm at the lower bound.

which explains why they tend towards thinner coatings. This, however, does not take into account that this also intensifies the sidebands in the focal plane and thus impairs the performance of the lens. Additionally, when comparing with figure 10, the minimum of the objective function should lie around 28 nm. Probably, for the thickness d at this point, an even lower d_c was more desirable for the swarm. That suggests interplays between the thickness of the ridges and of the coating. It also implies the influence of local minima on the PSO.

As a consequence of figures 10 and 11, the coating thickness in the final design was set to 35 nm. This leaves some space for deviations of the coating thickness while still making sure that SPPs will not couple into the gap easily. In general, when increasing the coating thickness, the design will eventually converge into the classic plasmonic lens design, consisting of a solid metallic slab with embedded dielectric waveguides. Keeping this in mind, it is preferable to fabricate the lens with a too thick coating rather than risking a too thin coating that enables unintended interactions.

Table 1. Best thicknesses for the fabrication of the inverted plasmonic lenses, chosen between 200 nm, 300 nm, 400 nm, 500 nm, and 600 nm, concerning the intensity of the focal spot.

λ_0/f	5 µm	10 µm	100 µm	1000 µm
455 nm	200 nm	200 nm	200 nm	200 nm
532 nm	200 nm	200 nm	200 nm	200 nm
632 nm	300 nm	200 nm	200 nm	200 nm
1064 nm	400 nm	200 nm	300 nm	300 nm
1550 nm	600 nm	600 nm	500 nm	500 nm

3.3. Ridge arrangement

In the past, plasmonic lenses were usually designed with periodic arrays of slits differing either in width [4], in depth [30] or even in refractive index of the dielectric [31]. However, using a periodic arrangement of the slits results in large areas with no slits at all because the slits at these positions would be so large that they would overlap with adjacent slits. This significantly decreases the possible throughput of the lens and, by this, the overall intensity of the focal spot. For this reason, an aperiodic placing of the ridges is also considered. We call this kind of arrangement successive because each ridge will be placed at the first possible position that allows it to be as wide as it needs while still leaving room for the metallic coating and a gap to the adjacent ridges. The simulation results of the inverted lens design show about twice as large intensities of the focal spots for the successive design compared to the periodic case. Therefore, aperiodic lens designs should be preferred.

3.4. Aperture

Concerning the aperture, a parameter space between 20 and 100 µm was set for the optimization. Figure 8 contains the first and last iterations of the respective PSOs. As briefly mentioned in section 3.1, the particles collect at the upper bound of the parameter space. Similar to the case of the coating thickness, larger apertures seem to be more beneficial in general, so the optimum lies outside of the parameter space. Lenses with a larger aperture have more space for ridges. This influences the focal spot as far as more ridges mean more throughput and therefore higher overall intensity. This explains the bunching of the particles at 100 µm. Overall, the aperture did not affect the influence of the thickness on the performance of the lens.

When we compare a plasmonic lens to a conventional lens, we might take a look at the numerical aperture (NA). A plasmonic lens can create a focal spot at a distance as close as 5 or 10 µm while presenting an aperture of 50 or 100 µm. This leads to numerical apertures well above one, namely between 2.5 and 10. However, it is debatable if the concept of the numerical aperture is applicable to plasmonic lenses.

4. Lens designs and tolerances

Based on the results presented in this contribution, a set of inverted plasmonic lenses was designed to later compare the simulations to measurements. The considered wavelengths and focal lengths are collected in table 1. Lenses with different

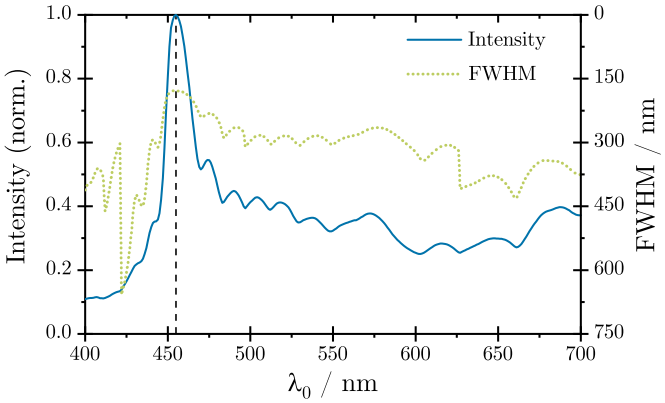

Figure 12. Intensity (blue, solid) and FWHM (green, dotted) in dependence of the wavelength. The design wavelength 455 nm is indicated by the dashed black line. There, the lens has a bandwidth of about 31 nm.

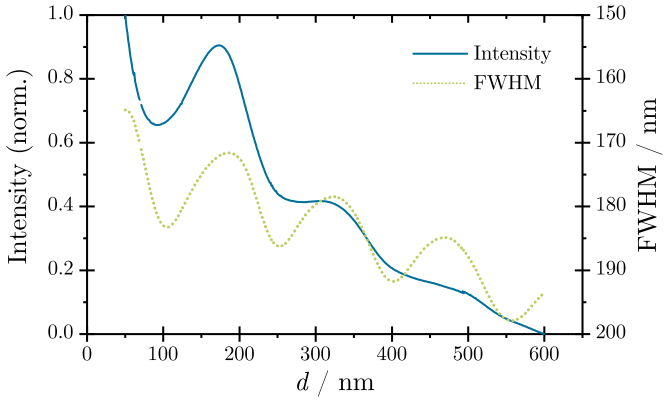

Figure 13. Intensity (blue, solid) and FWHM (green, dotted) of the focal spot of a lens with fixed slit positions and widths for different thicknesses d. The parameter set was computed beforehand for $d = 200$ nm.

thicknesses are hard to fabricate on the same wafer. Therefore, for each of the aimed parameter sets, the corresponding lens was designed for five different thicknesses between 200 nm and 600 nm with fixed ridge parameters to find two thicknesses that work best for each design in terms of focal spot intensity. The results are also presented in table 1. Clearly, lenses for larger wavelengths also work better with larger thicknesses due to the corresponding longer SPP wavelength. Most of the lenses for shorter wavelengths worked best for $d = 200$ nm. Thus, for each parameter set, two lenses were fabricated with $d = 200$ nm and 600 nm, respectively. Additionally, in our simulations, we also filled the gaps between the ridges with resists for enhanced stabilization of the structures.

4.1. Wavelength tolerance

Inverted plasmonic lenses for arbitrary wavelengths of the incident light can be designed, but due to the plasmonic nature of the lenses, they only work at the specified wavelength for which they were designed. Figure 12 shows the intensity and FWHM of a lens that was designed for a wavelength of 455 nm for different incident wavelengths in the visible range. The lens reaches its maximum of intensity at the design wavelength. For smaller or larger wavelengths, the intensity decreases rapidly and lies below 50% of its maximum over the whole visible range. The bandwidth of the lens is about 31 nm. For this reason, plasmonic lenses could also be thought of as bandpass filters with a narrow band. In addition, the FWHM reaches its minimum also at the design wavelength, resulting in the smallest focal spot at 455 nm.

4.2. Thickness tolerance

As presented in section 3.1, optimizing only the thickness of the lens without recomputing the ridge parameters each time reveals an ideal thickness below the one for which the lens was initially designed. The blue solid curve in figure 13 shows the intensity of the focal spot of an inverted plasmonic lens for different thicknesses, but with fixed ridge parameters. As the ridge widths now stay the same, as opposed to in figure 6, the overall intensity decreases with the thickness, because SPPs decay during their propagation. Simultaneously, the FWHM illustrated by the green dotted line in figure 13 increases with the thickness as the spot slightly broadens. The lens is physically realizable even for thicknesses larger than λ_c because this limit only applies to the mathematical model that is used to compute the ridge parameters. So the ridge widths and positions should be determined for a thickness between λ_{SPP} and λ_c, as stated in section 3.1, but the optimization of the lens's final thickness should be performed with this fixed set of parameters instead of re-evaluating equation (2) each time to reach an optimal performance.

The periodicity in the curves in figure 13 leads back to the phase shift induced by the varying thickness that causes a small periodic shift of the focal length. By this, the focal spot shifts in and out of the observed plane at the expected focal length, which influences the perception of the spot's intensity and especially its FWHM. However, thickness deviations smaller than about 50 nm do not dramatically affect the performance of the lens.

4.3. Estimation of statistical deviations from design

To examine how statistical deviations in the fabrication process might influence the performance of the lens, we simulated a lens with $d = 300$ nm at $\lambda_0 = 532$ nm and manipulated the position of each ridge with a random displacement. Figure 14 shows the intensity of the focal spot of the lens for different scales σ of the Gaussian distributed random displacement. The scale σ represents the standard deviation of the Gaussian distribution used to determine the displacement values. As this is a statistical problem, a thorough investigation would obviously need several runs to yield exact results. However, as figure 14 shows, even with only one run of randomly displacing the ridges with increasingly larger values, we can observe a

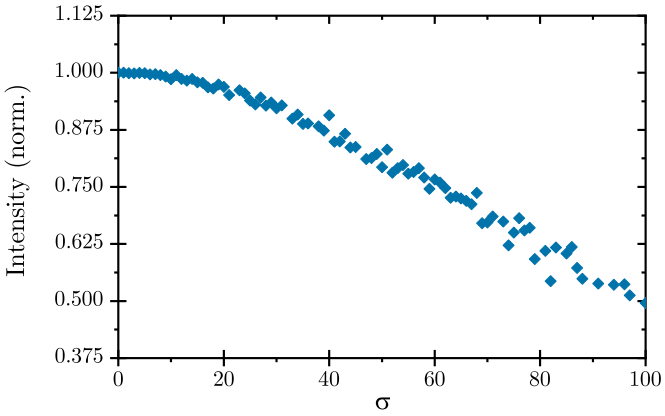

Figure 14. Intensity of a lens for differently scaled randomly distributed displacements of the ridges.

significant drop in the intensity of the focal spot. Nevertheless, for σ up to 10, the intensity is barely influenced by the displacement, so the fabrication of the lenses is not required to match the design of the arrangement down to less than about 50 nm.

5. Conclusion

In this contribution, we presented a new plasmonic lens design, called the inverted plasmonic lens. Instead of travelling through slits in a metallic slab, in the inverted design SPPs propagate through dielectric ridges with metallic sidewalls. For the computation of the widths and positions of the plasmonic ridges on the lens, the height of the ridges (i.e. thickness of the lens) between the wavelength of the SPPs and λ_0/n_d should be used. Particle swarm optimization for the thickness with fixed parameter sets for widths and positions revealed that optimal performance of the lens is achieved for thicknesses well below the thickness for which they were designed. Additionally, coating thicknesses larger than or equal to 35 nm are recommended, as well as an aperiodic placement of the ridges to achieve a higher intensity of the focal spot. Inverted plasmonic lenses with focal spots between 5 μm and 1 mm were designed and discussed. The achieved design enables the simplified fabrication of several hundred plasmonic lenses in a few hours using electron beam lithography techniques. The production time could be reduced even more when using nanoimprint lithography.

Acknowledgments

This work is funded through the project 17FUN01 "BeCOMe" within the Programme EMPIR. The EMPIR initiative is co-founded by the European Union's Horizon 2020 research and innovation program and the EMPIR Participating Countries.

ORCID iD

T Käseberg https://orcid.org/0000-0003-1389-5117

References

[1] Fang N, Lee H, Sun C and Zhang X 2005 Sub-diffraction-limited optical imaging with a silver superlens *Science* **308** 534–7
[2] Shi H, Wang C, Du C, Luo X, Dong X and Gao H 2005 Beam manipulating by metallic nano-slits with variant widths *Opt. Express* **13** 6815–20
[3] Xu T, Du C, Wang C and Luo X 2007 Subwavelength imaging by metallic slab lens with nanoslits *Appl. Phys. Lett.* **91** 201501
[4] Fu Y and Zhou X 2010 Plasmonic lenses: a review *Plasmonics* **5** 287–310
[5] Srituravanich W, Pan L, Wang Y, Sun C, Bogy D B and Zhang X 2008 Flying plasmonic lens in the near field for high-speed nanolithography *Nat. Nanotechnol.* **3** 733
[6] Peng R, Li X, Zhao Z, Wang C, Hong M and Luo X 2014 Super-resolution long-depth focusing by radially polarized light irradiation through plasmonic lens in optical meso-field *Plasmonics* **9** 55–60
[7] Catrysse P B, Verslegers L, Yu Z, White J S, Barnard E S, Brongersma M L and Fan S 2009 Nanoscale slit arrays as planar far-field lenses *Proc. SPIE 7394, Plasmonics: Metallic Nanostructures and Their Optical Properties VII*, 73940B
[8] Hell S W and Wichmann J 1994 Breaking the diffraction resolution limit by stimulated emission: stimulated-emission-depletion fluorescence microscopy *Opt. Lett.* **19** 780–2
[9] Rust M J, Bates M and Zhuang X 2006 Stochastic optical reconstruction microscopy (storm) provides sub-diffraction-limit image resolution *Nat. Methods* **3** 793
[10] Rothen A 1945 The ellipsometer, an apparatus to measure thicknesses of thin surface films *Rev. Sci. Instrum.* **16** 26–30
[11] Losurdo M 2011 Applications of ellipsometry in nanoscale science: needs, status, achievements and future challenges *Thin Solid Films* **519** 2575–83
[12] Kerwien N 2007 On the influence of polarization effects in microscopic image formation Ph.D. thesis Institute of Applied Optics, University of Stuttgart (http://dx.doi.org/10.18419/opus-4130)
[13] Käseberg T, Dickmann J, Siefke T, Wurm M, Kroker S and Bodermann B 2019 Mueller matrix ellipsometry for enhanced optical form metrology of sub-lambda structures *Proc. SPIE 11057, Modeling Aspects in Optical Metrology VII*, 110570R
[14] Jahns J and Helfert S 2012 Introduction to Micro-and Nanooptics (New York: Wiley)
[15] Raether H 1988 Surface plasmons on smooth and rough surfaces and on gratings *Springer Tracts Mod. Phys.* **111** 1
[16] Barnes W L 2006 Surface plasmon-polariton length scales: a route to sub-wavelength optics *J. Opt. A: Pure Appl. Opt.* **8** S87
[17] Gordon R and Brolo A G 2005 Increased cut-off wavelength for a subwavelength hole in a real metal *Opt. Express* **13** 1933–8
[18] Chen W, Abeysinghe D C, Nelson R L and Zhan Q 2009 Plasmonic lens made of multiple concentric metallic rings under radially polarized illumination *Nano Lett.* **9** 4320–5
[19] Liu Y, Xu H, Stief F, Zhitenev N and Yu M 2011 Far-field superfocusing with an optical fiber based surface plasmonic lens made of nanoscale concentric annular slits *Opt. Express* **19** 20233–43
[20] Li H, Fu L, Frenner K and Osten W 2018 Cascaded plasmonic superlens for far-field imaging with magnification at visible wavelength *Opt. Express* **26** 10888–97
[21] Blaber M G, Arnold M D and Ford M J 2010 A review of the optical properties of alloys and intermetallics for plasmonics *J. Phys.: Condens. Matter.* **22** 143201

[22] Johnson P B and Christy R W 1972 Optical constants of the noble metals *Phys. Rev.* B **6** 4370–9
[23] West P R, Ishii S, Naik G V, Emani N K, Shalaev V M and Boltasseva A 2010 Searching for better plasmonic materials *Laser Photonics Rev.* **4** 795–808
[24] Siefke T, Lehr D, Weber T, Voigt D, Kley E B and Tünnermann A 2014 Fabrication influences on deep-ultraviolet tungsten wire grid polarizers manufactured by double patterning *Opt. Lett.* **39** 6434–7
[25] Lehmuskero A, Kuittinen M and Vahimaa P 2007 Refractive index and extinction coefficient dependence of thin Al and Ir films on deposition technique and thickness *Opt. Express* **15** 10744–52
[26] Weber T, Käsebier T, Kley E B and Tünnermann A 2011 Broadband iridium wire grid polarizer for UV applications *Opt. Lett.* **36** 445–7
[27] JCMsuite 2019 *The Simulation Suite for Nano-Optics Jcmwave Gmbh* JCMsuite Berlin (available at: https://www.jcmwave.com/) (Accessed: 20 November 2019)
[28] Kennedy J and Eberhart R 1995 Particle swarm optimization *Proc. of ICNN'95—Int. Conf. on Neural Networks* vol 4 pp 1942–8
[29] Clerc M and Kennedy J 2002 The particle swarm-explosion, stability, and convergence in a multidimensional complex space *IEEE Trans. Evol. Comput.* **6** 58–73
[30] Shi H and Jay Guo L 2010 Design of plasmonic near field plate at optical frequency *Appl. Phys. Lett.* **96** 141107
[31] Chen Q 2011 Effect of the number of zones in a one-dimensional plasmonic zone plate lens: simulation and experiment *Plasmonics* **6** 75–82